中國機械工程學刊第四十六卷第二期第 131~140 頁(民國一百一十四年)
Journal of the Chinese Society of Mechanical Engineers, Vol.46, No.2, pp 131~140 (2025)

Numerical Simulation of Permeability for Novel Lattice Structures Under Various Flow Conditions

Parth Goyal*, Senthilkumar S* and Kang Shung-Wen**

Keywords: - Porous Media, Permeability, Lattice structures, Porosity, Re, Lateral Length.

ABSTRACT

Porous materials are essential in applications like impact absorption, thermal management, tissue engineering, and vibration damping, making their detailed study crucial. Key parameters in pore structure characterization include porosity, pore distribution, types, aperture size, shape, tortuosity, pore size distribution, specific surface area, and permeability. This study numerically simulates the permeability of two Triply Periodic Minimal Surfaces (TPMS) structures—Primitive and Gyroid—and two strut-based lattice structures—Diamond and Iso-truss. The analysis was conducted under steady-state conditions, with variations in porosity levels (60%, 70%, 80%, 90%), Reynolds numbers (Re) of 10, 50, 100, 150, 200, and 250, and a lateral length of 3 mm. Results indicate that higher porosity correlates with higher permeability, while increasing Re lead to higher pressure drops, reducing permeability. Among the structures, the lattice Diamond shows the highest permeability, while TPMS Primitive generally has the lowest.

INTRODUCTION

In today's engineering porous structure plays a very vital role. Porous media is used in various areas of science and engineering fields for example filtration, mechanics, engineering, geosciences, biology, fuel cells, food production, and drying of pulp and paper. The Scientific study of porous structures was started in the 18th century, Reint (1996) and today it has been well-established to use porous materials because of its better strength, heat and fire resistance and its lightweight properties. Traditionally, the characterization of pore structure involves parameters such as porosity (the volume fraction of all pores), spatial distribution of pores, pore types (open, closed, etc.), aperture size (fraction of cross-sectional area of channels), shape and tortuosity coefficients of pores, pore size distribution, specific surface area, permeability, and its distribution across the filtration area (Dias et al. 2012; Pennella et al. 2013). Z. Sarparast et al. Sarparast et al. (2020) explore the influence of scaffold microstructure permeability, examining different pore sizes and porosity levels. Results demonstrated a positive relationship between porosity and permeability, indicating that higher porosity led to increased permeability. Furthermore, the study found that larger pore sizes correlated with higher permeability, suggesting that adjusting pore size alone could enhance permeability for scaffolds with consistent porosity levels. Ahmed et al. (2011) focused on numerical analysis of heat pipes, examining key factors such as porosity, heat flux, pipe length, wall thickness, and material composition. Findings indicated that porosity significantly influences heat pipe performance, with higher porosity levels correlating to elevated wall temperatures, while lower porosity levels resulted in the lowest wall temperatures. Zhu et al. (2021) analyse the influence of capillary number (Ca), viscosity ratio (M), and wettability on permeability curves in three-phase fluid flow through a 3D porous medium with small porosity and low pore size. They employed the Lattice Boltzmann colour gradient model to investigate this phenomenon. Validation of their results was carried out by comparing them with parameters from other studies, including multiphase spinodal decomposition, the multiphase Young-Laplace test, liquid lens behaviour, contact angle

Paper Received August, 2024. Revised October, 2024. Accepted November, 2024. Author for Correspondence: Shung-Wen Kang.

Department of Aerospace Engineering, SRM Institute of Science and Technology, Kattankulathur, Chennai, India – 603203

**Department of Mechanical and Electro-Mechanical Engineering, Tamkang University, Tamsui Dist., New Taipei City, Taiwan (R.O.C) – 251301*

measurements, and three-dimensional channel-layered three-phase fluid flow analysis. Their findings says that as wettability increases, the permeability of the non-wetting phase rises while that of the wetting phase decreases. When the viscosity ratio deviates from unity, the relative permeability of the phase with higher viscosity experiences a notable increase, while the permeability of the other two phases is less affected. Moreover, with an increase in the capillary number, the relative permeability initially increases before stabilizing at a steady state.

Lattice structures are three-dimensional design components made up of repeating unit cells at the meso-level. Due to easy designing, lattice structures have been analysis in various research fields in which they have showed good light-weighting and stiffness, deformation behaviour [7] which can be used in aerospace industry, biomedical and energy adsorbing application (Bicia et al. 2018). Ali et al. (2020) investigatede on different architectures with gyroid and lattice-based rectangular unit cells. Their results reveal that lattice-based module shows higher elastic modulus, compressive strength and permeability in rectangular lattice bases structure. Lattice structures come in 2.5D (Fan et al. 2007) or 3D configurations and can be manufactured using various methods, including investment casting (Kooistra et al. 2004), a combination of extrusion and electro-discharge machining (Queheillalt et al. 2008) or composite fabrication techniques like textile weaving (Fan et al. 2013), interlacing, interlocking, hot-pressing (Fan et al. 2010) or filament winding (Li et al. 2016). Since the advent of Additive Manufacturing (AM) in the late 1990s and early 2000s (Wohlers et al. 2015), there has been a notable shift in research focus towards the AM fabrication of lattice structures (Dong et al. 2017). Particularly, Selective Laser Melting (SLM) has garnered significant attention for its advantages in producing metallic lattice structures (Leary et al. 2016). Numerous studies have investigated the properties of lattice structures fabricated via SLM. Strut-based lattice structures consist of interconnected rod-like forms arranged in different orientations to form distinct unit cells. The most commonly researched strut-based cell topologies include the Body-Centered Cubic (BCC) and Face-Centered Cubic (FCC), as well as variations such as those incorporating Z-struts (BCCZ and FCCZ) (Maskery et al. 2017), named in analogy to crystalline structures. Additionally, other strut-based topologies like cubic, octet-truss, and diamond configuration also exist.

TPMS are defined as mathematical surfaces which are characterized by having zero mean curvature, implying that the sum of the principal curvatures at every point equal zero (Ai-Ketana et al. 2018). TPMS structures minimize their surface area while having fixed boundary curves, resulting in smooth and continuous surfaces characterized by low-density geometry. These unique properties make TPMS structures highly desirable and widely utilized in various applications, including biological membranes and biphotonic structures such in butterfly-wing scales (Schröder-Turk et al. 2018), urchins, some liquid crystals and in heat exchanger such as heat pipes (Attarzadeh et al. 2021), that’s why it becomes more important to study about TPMS structures. The concept of TPMS was first discovered by Schwarz in 1865 and further worked upon by his student Neovius (1883), they identified five unique TPMS structures: Schwarz Primitive, Schwarz Diamond, Schwarz Hexagonal, Schwarz Crossed Layers of Parallels and Neovius. Then, the most famous gyroid surface was described by in 1970, along with another eleven newly discovered TPMS (Schoen, 1970). In numerous studies, TPMS have demonstrated their capacity for acoustic (Wang and Lu, 1999)] and vibrational damping (Göransson, 2006), along with their effectiveness in absorbing compressive energy (Stupak and Donovan, 1994), while also exhibiting excellent thermal and physical properties (Klinowski et al. 1996). TPMS and related surfaces can be approximately visualized by the nodal equations in terms of the Fourier series using the structure factor $F(\mathbf{k})$ with a given reciprocal lattice vector $\mathbf{k}$ and the phase shift $\alpha(\mathbf{k})$ shown in Eq. (1) (Jung et al. 2007).

$$\boldsymbol{\Psi}(\mathbf{r}) = \sum_{\mathbf{k}} F(\mathbf{k}) \cos\left[2\pi \mathbf{k}.\mathbf{r} - \alpha(\mathbf{k})\right] = 0 \qquad (1)$$

Approximations of the TPMS can be obtained by truncating the series which gives the required geometries, Gyroid, Diamond and Primitive surface in simple expressions respectively:

$$\sin X \cos Y + \sin Z \cos X + \sin Y \cos Z = t \qquad (2)$$

$$\cos X \cos Y \cos Z - \sin X \sin Y \sin Z = t \qquad (3)$$

$$\cos X + \cos Y + \cos Z = t \qquad (4)$$

Where $X = 2\pi x/a$, $Y = 2\pi y/a$, $Z = 2\pi z/a$, and a is the unit cell parameter. The most challenging processes in designing TPMS structures is manufacturing TPMS geometries but Additive manufacturing technology has made itself as an ideal solution for the fabrication of intricate TPMS porous structures (Wong and Hernandez, 2012). Various processes have been attempted to manufacture TPMS porous structures, including SLM (Yan et al. 2015), selective laser sintering (SLS) (Al-Ketan, 2019), Stereo Lithography Apparatus (SLA) (Yu et al, 2019), digital light processing (DLP) (Yao et al.

2021), fused deposition modelling (FDM) (Maconachie et al., 2020). TPMS geometries exhibit a high surface-to-volume ratio, improved pore connectivity, and translational symmetry along three distinct axes (x, y, and z directions).

Zhianmanesh et al. (2019) investigated the impact of fluid permeability focusing on scaffolds constructed using Primitive, Gyroid, IJ*-P2 and F_{xyz}-F_{xxx}2 TPMS. The findings indicate that the relationships between permeability and gradient parameters can vary based on pore shape and Primitive showed more permeability except approximate at 30% porosity where Gyroid has higher permeability and Fxyz-Fxxx2 and IJ*-P2 were the less permeable structures. Rathore et al. (2023) focused on three different zones and used four TPMS structures and there finding has showed that the maximum and minimum permeability values were observed in Primitive Type 2 and I-WP Type 1 lattices, respectively. Generally, Type 2 lattices exhibited the highest permeability values and the lowest inertial drag factors, resulting in the lowest pressure drop. Santos et al. (2020) employed three distinct TPMS structures—Schwartz Diamond, Gyroid, and Schwartz Primitive across four porosity levels (50%, 60%, 70%, and 80%). Their results show that Schwartz Diamond showed least permeability and Schwartz Primitive showed the most permeability. Ali et al. (2020) showed that lattice diamond has maximum permeability whereas double diamond has minimum permeability out of eight geometries that they choose and overall lattice showed better permeability then TPMS except octet and truncated octahedron which had less permeability than gyroid. Li et al. (2024) compared IWP and Primitive TPMS structures and the results indicated that primitive have better permeability then IWP. Montazerian et al. (2017) studied on longitudinal and radial permeability of lattice and TPMS structures and their results showed that in lattice hexagonal and in TPMS I-WP showed better permeability and also radial is better than longitudinal permeability. Castro et al. (2019) investigated the influence of porous TPMS structures on permeability behaviour and their findings indicate that the Gyroid scaffold exhibits superior permeability, while the Schwartz Primitive structure demonstrates a lower likelihood of fluid flow and Schwartz Diamond yielded less favourable results in terms of permeability. Guisheng et al. (2020) studied on compressive, tensile, and permeability properties using experimental and numerical of the porous scaffolds which were Primitive, Gyroid and BCC with 65% porosity. Their results showed that Gyroid had better compressive strength and tensile strength, 2 time higher than BCC structure and in permeability it showed opposite result, BCC been highest permeable and Gyroid been the least. Attarzadeh et al. (2021) investigated on heat exchanger and permeability of Schwartz D numerically. They varied the cell thickness and at different Re. Their results showed that having less thick wall will have more heat exchange, the thermal performance of least thick wall was 250% better than the wall with most thickness in their research.

From the available data given in literature it can be seen, that a lot of work has been done in permeability on various strut-based and TPMS lattice structures but there has been a gap in knowledge with these structures. This research by numerical simulation try to fill the gap by choosing Iso-truss lattice structure which has been least studied for permeability and choosing different range of Re (10, 50, 100, 150, 200, 250) and porosity (60%, 70%, 80%, 90%) on TPMS Gyroid, Schwartz Primitive, Strut-based Diamond and Iso-truss structures which has been the studied less.

METHODOLOGY

CFD Simulation and Governing Equations

ANSYS FLUENT is used to solve the 3D incompressible Navier-Stoke equations, including

Continuity equation:

$$div(\boldsymbol{u}) = 0 \tag{5}$$

x-momentum equation:

$$div(u\boldsymbol{u}) = -\frac{\partial p}{\partial x} + \nu\, div(grad\ u) \tag{6}$$

y-momentum equation:

$$div(v\boldsymbol{u}) = -\frac{\partial p}{\partial y} + \nu\, div(grad\ v) \tag{7}$$

z-momentum equation:

$$div(w\boldsymbol{u}) = -\frac{\partial p}{\partial z} + \nu\, div(grad\ w) \tag{8}$$

continuity equation Eq. 5 and momentum equations Eqs. 6-8 of the fluid flow assuming steady and laminar state.

The simulations were done to find the total pressure difference of the lattice structure in the fluid domain which was taken as difference between the inlet and outlet of the fluid domain. The pressure difference was used to insert in Darcy's Law to find the permeability: -

$$q = \frac{Q}{A} = \left(\frac{k}{\mu L}\right) \times \Delta\text{p} \tag{9}$$

Method Validation for Pressure Drop and Permeability

Validating a numerical model is an essential step in the simulation process as it establishes confidence in the model's ability to produce accurate results. For validation, the outcomes of the numerical model were compared with those reported in the research paper by Jafari et al. (2018). Specifically, the pressure drops and permeability values from the study were used as benchmarks. The geometry used for validation, depicted in Fig. 1, was recreated in nTopology and is analogous to that described in the paper. The geometry dimensions are 8×8×16 mm with cell dimensions of 2×2×2 mm. The fluid domain extends to 8.1×8.1×20 mm, providing an additional 4 mm to ensure fluid stability and steadiness. The boundary conditions mirror those in the reference paper, utilizing water with a density of 998.2 kg/m3 and a viscosity of 0.001 Pa. The flow is steady-state and laminar, with inlet velocities set at 0.01, 0.008, 0.006, 0.004, 0.002, and 0.001 m/s, and an outlet pressure of 0 Pa. All other surfaces are treated as walls with a no-slip condition.

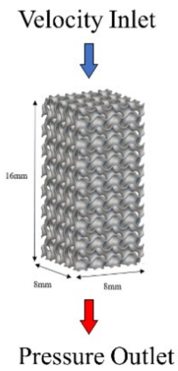

Fig.1 Geometry of porous structure.

Figure 2(a) shows the pressure drop graph from the research paper results and the numerical model results for Gyroid structure is shown in Fig. 2(b). From Fig. 2, it is clear that the numerical model shows a good agreement with the research paper results. Figure 3 shows the permeability value from the research paper and the calculation shown below which is used to calculate the permeability from the numerical model also show good agreement with each other.

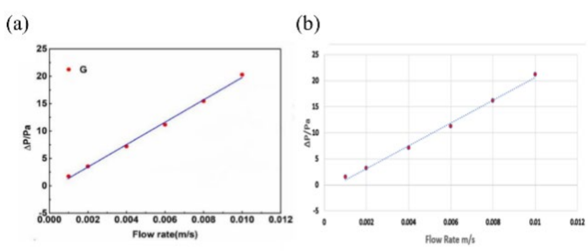

Fig.2 (a) Pressure drop from [43].

(b) Pressure drop from this study.

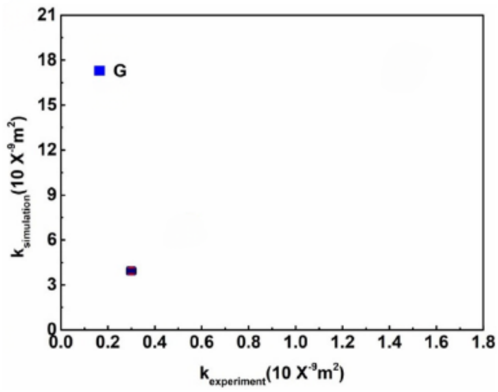

Fig. 3 Permeability from [43]

Darcy's Law's Eq. (9) was used to calculate the permeability (k) using the numerical results for the simulation conditions with Q= 6.7×10^{-7} m^3/s, A = 6.4×10^{-5} m^2, μ= 0.001 kg/(m s) , L= 0.016 m, Δp = 21.21 Pa and, and k=3.95×10^{-9} m^2. Hence, from these two results namely both pressure drop and permeability values, it can be said that the numerical model agrees well with those of the reference paper.

Geometry Design

For creating the design of lattice structures using conventional CAD software is not advisable because it takes a lot of processing power and time to create the designs for them. The software used for the lattice creation is nTopology, which can create the complex structure specially lattice within a fraction of the time. nTopology is one of the best ways to create geometrical structures with better resolution as well. The structures used were TPMS Gyroid, TPMS Primitive, Strut-based Diamond and Iso-truss of 3×5×5 mm as shown Fig. 4. The cell unit size was 1×1×1 mm, 3mm lateral length was taken, for fluid to archive steady state 5 mm space was given for fluid domain as shown in Fig. 5. Measuring porosity was also done in nTopology using its weight saving function in which it divides the volume of void structure to the original total volume of non-void structure.

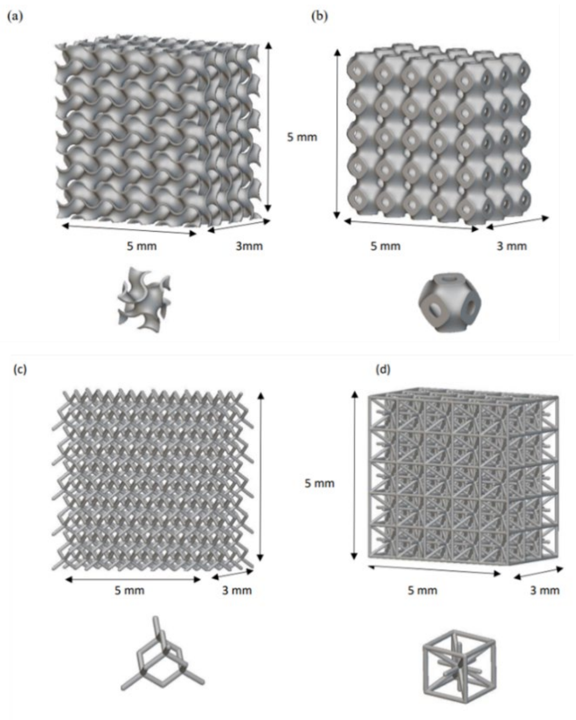

Fig. 4 Lattice structures: (a) TPMS Gyroid (b) TPMS Primitive (c) Diamond (d) Iso-Truss.

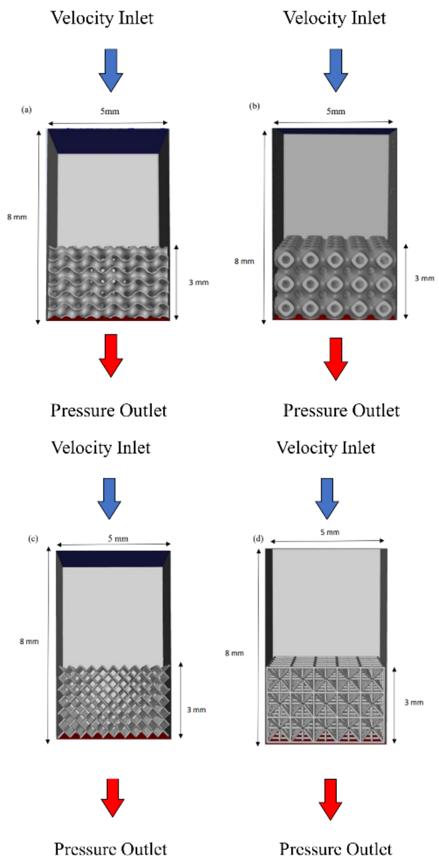

Fig. 5 Fluid domain for (a) TPMS Gyroid (b) TPMS Primitive (c) Diamond (d) Iso-Truss.

Method and Boundary Conditions Applied

The water (ρ = 998.2 kg/m^3, μ = 0.001003 kg/m·s) was chosen as the fluid of the medium which was selected from the ANSYS database. The boundary conditions are applied on one surface as velocity inlet, one surface as pressure outlet and rest of the surfaces act as wall with no slip condition. The velocity was calculated using Re formula Eq. 10 and since Darcy's law is applicable only in laminar region, therefore the Re were selected as Re = 10, 50, 100, 150, 200, 250 and it was calculated using:

$$Re = \frac{\rho u D_h}{\mu} \tag{10}$$

For residual the continuity equation and momentum equations were set as 1×10^{-6}. The SIMPLE scheme, least square cell based spatial discretization, second order pressure and second order upwind were applied for all the simulations.

Mesh Generation

After creating the geometry, the next step involves generating a volume mesh, which discretizes both the interior and exterior surfaces of the object, unlike surface mesh that only covers the exterior. For this task, nTopology was employed due to its efficiency and time-saving capabilities compared to other software.

Grid Independence Study

Validating grid independence is essential for the project because while a finer mesh improves simulation accuracy, overly fine meshes increase computational time. By systematically refining the mesh and evaluating the results, it's possible to identify the optimal mesh size that provides consistent and convergent outcomes. Once the mesh size reaches a point where output changes are minimal, further refinement is unnecessary and should be avoided to simplify the solution and decrease runtime. Figure 6 illustrates a mesh independence study for each structure, conducted with up to 1000 iterations per case to achieve stable and converged numerical solutions.

For the grid independence study, the boundary conditions were as follows: an inlet velocity of 0.001 m/s to maintain laminar flow, a pressure-outlet of 0 Pa at the output, and the remaining four surfaces treated as walls. As shown in Fig. 6, while increasing mesh cell numbers initially leads to variations in permeability values, these values eventually stabilize, albeit at the cost of increased computation time. Consequently, the most optimal mesh cell numbers were selected to balance accuracy and efficiency. The range of mesh cell numbers for each lattice structure is specified in Table 1.

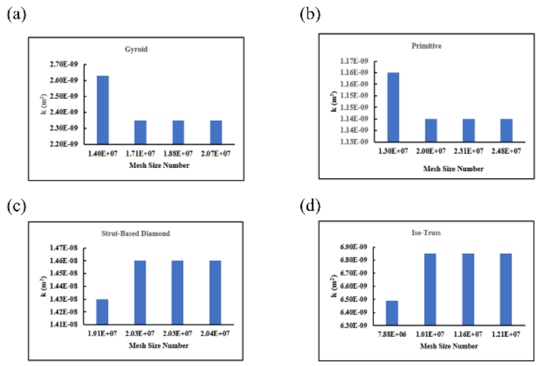

Fig. 6 Mesh Independence Study of (a) Gyroid (b) Primitive (c) Strut-Based Diamond (d) Iso-Truss.

Table 1 Mesh cell numbers for TPMS structures

S. No.	LATTICE STRUCTURES	MESH CELL NUMBERS RANGE
1	TPMS Gyroid	(17.15 – 20.71) × 10^6
2	TPMS Primitive	(20.05 – 24.78) × 10^6
3	Strut-Based Diamond	(20.30 - 20.40) × 10^6
4	Iso-Truss	(20.30 - 20.40) × 10^6

RESULTS

Numerical simulations were conducted on Gyroid, Primitive, Strut-Based Diamond, and Iso-truss structures at porosities of 60%, 70%, 80%, and 90% across Res 10, 50, 100, 150, 200, and 250. The results are presented in plots comparing Pressure Difference and Permeability against Re, as well as against different lattice structures at constant porosities.

Pressure Difference vs Re of Lattice Structures

Figure 7 displays graphs of pressure difference versus Re for various lattice structures at different porosity levels. The graphs indicate that pressure difference rises with increasing Re and that lattice structures with lower porosity exhibit higher pressure differences across all Res. The TPMS Primitive shows the highest pressure gradient, while the Strut-Based Diamond exhibits the lowest compared to other structures. At a Re of 10, the minimum pressure difference is observed in all cases.

(a)

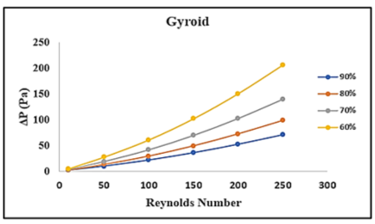

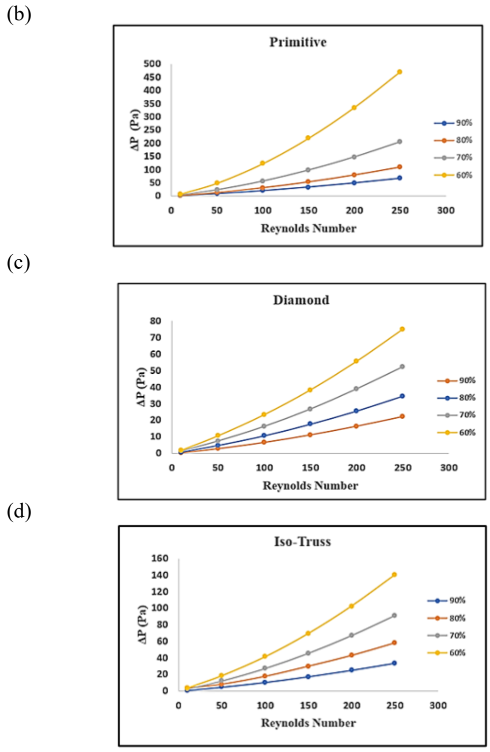

Fig. 7 Pressure difference vs Re of (a) Gyroid (b) Primitive (c) Strut-Based Diamond (d) Iso-Truss

Permeability vs Re of Lattice Structures

Figure 8 shows the variation of permeability with Re of lattice structures for various porosity values. From the graphs, it can be seen that the permeability of all the structures decreases with increase of Re, and at all the Re and porosity the strut-based diamond as shown the most and Iso-Truss the second most permeable structures out of all the discussed structures. At 90% and 80% porosity, the TPMS Primitive structure exhibits higher permeability compared to the TPMS Gyroid. However, at 70% and 60% porosity, the TPMS Gyroid demonstrates greater permeability than the TPMS Primitive.

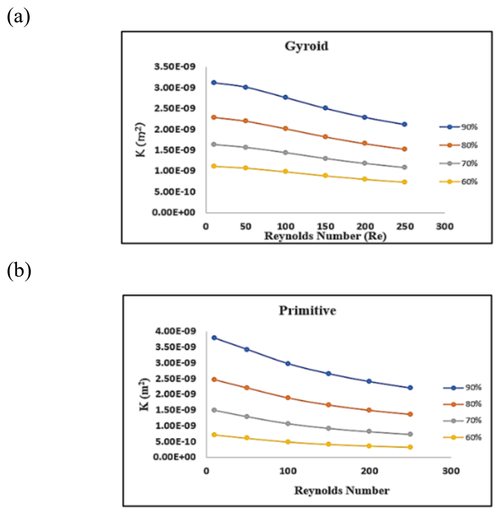

(c)

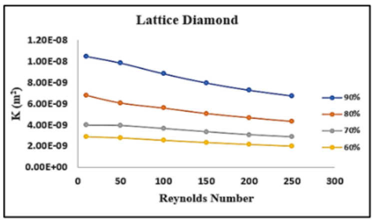

(d)

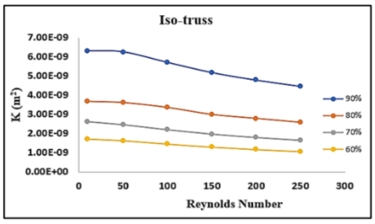

Fig. 8 Permeability vs Re of (a) Gyroid (b) Primitive (c) Strut-Based Diamond (d) Iso-Truss

Pressure Drop vs Lattice Structure at fixed porosity

Figure 9 illustrates the pressure differences across various lattice structures at different porosities. It is evident that TPMS Primitive consistently exhibits the highest-pressure differences across most porosities, with TPMS Gyroid slightly edging it out at 90% porosity. Conversely, both Strut-Based Diamond and Iso-Truss structures consistently demonstrate lower pressure differences. This suggests a general trend: Strut-Based structures exhibit lower pressure differences compared to TPMS structures in the analysis. These findings underscore the comparative advantage of Strut-Based Structures in minimizing pressure differentials.

(a)

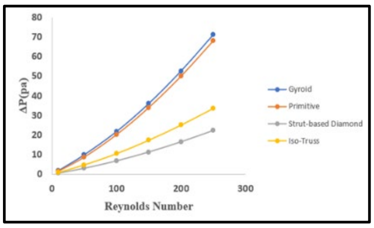

(b)

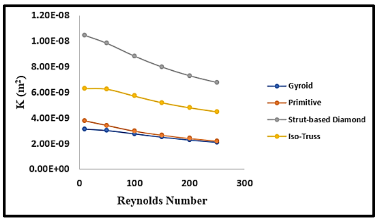

(c)

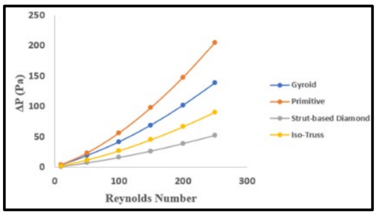

(d)

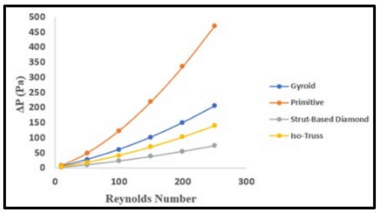

Fig. 9 Pressure difference vs Re of Lattice structures at (a) 90% (b) 80% (c) 70% (d) 60%, Porosity.

Permeability vs Lattice Structure at fixed porosity

Figure 10 shows the variations of permeability for various Lattice Structures with 90%, 80%, 70%, 60% porosity values respectively. It is observed that the Strut-based Diamond is the most permeable than the rest of the Lattice Structures, Iso-Truss has also shown good results making it second most permeable structure. From Fig. 10(a) & 10(b), the TPMS Primitive at 90% porosity had slightly low-pressure difference as compared to the TPMS Gyroid due to which at 90% porosity the TPMS Primitive is slightly more permeable than that of TPME Gyroid but at 80%, 70% and 60% the TPMS Primitive has more pressure difference as compared to the TPMS Gyroid due to which, making it less permeable as compares to the TPMS Gyroid as well as with other Lattice Structures. This variation in the TPMS structure may be because the TPMS Gyroid has a greater number of holes than the TPMS Primitive. These results also show that the Strut-Based Structures have more Permeability than the TPMS Structures.

(a)

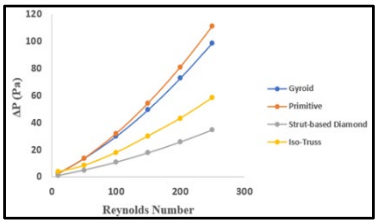

(b)

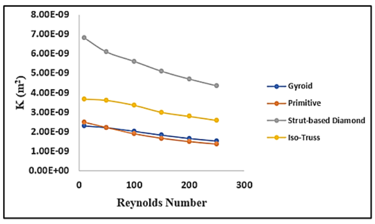

(c)

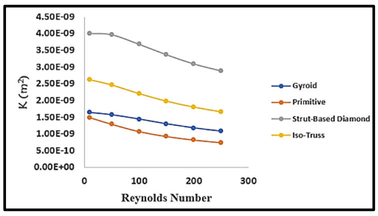

(d)

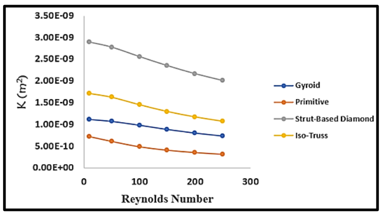

Fig. 10 Permeability vs Re of Lattice Structures at (a) 90% (b) 80% (c) 70% (d) 60%, Porosity.

CONCULSION

A numerical simulation was conducted to evaluate the permeability of various lattice structures—TPMS Gyroid, TPMS Primitive, Strut-based Diamond, and Iso-Truss—across Res (250, 200, 150, 100, 50, 10) and porosities (60%, 70%, 80%, 90%), totaling 96 scenarios. Results showed permeability levels of 10^{-8}, 10^{-9}, and 10^{-10}. The Strut-based Diamond exhibited the highest permeability (10^{-8}) at Re 10 with 90% porosity, while TPMS Primitive had the lowest (10^{-10}) at Re 250 with 60% porosity, highlighting an inverse relationship between permeability and Re. Iso-Truss performed well, ranking second in permeability, with TPMS Gyroid third except at 90% porosity, where TPMS Primitive was more permeable. These findings suggest strut-based structures generally offer higher permeability than TPMS structures. In terms of pressure difference, the results were reversed: pressure difference increased with Re. TPMS Primitive had the highest pressure difference except at 90% porosity, while Strut-based Diamond consistently showed low pressure differences. Thus, strut-based structures are preferable for applications requiring higher permeability.

ACKNOWLEDGEMENTS

Financial support for this work was provided by the National Science and Technology Council (NSTC), R.O.C, under the contract 112-2221-E-032 -026.

References

Ahmed, N. Z., Singh, P. K., Janajreh, I. and Shatilla, Y., "Simulation of flow inside heat pipe: sensitivity study, conditions and configuration." Proc. ASME Int. Conf. ESFuelCell, (2011).

Ali, D., Ozalp, M.,Blanquer, S. B. G. and Onel, S., "Permeability and fluid flow-induced wall shear stress in bone scaffolds with TPMS and lattice architectures: A CFD analysis." Eur. J. Mech. B Fluid., Vol. 79, pp. 376-385 (2020).

Al-Ketan, O., Reza Rowshan, R. and Al-Rub, R. K. A., "Topology-mechanical property relationship of 3D printed strut, skeletal, and sheet based periodic metallic cellular materials.", Addit. Manuf., Vol. 19, pp. 167-183 (2018).

Al-Ketan, O., Rowshan, R., Palazotto, A. N. and Al-Rub, R. K. A.,"On Mechanical properties of cellular steel solids with shell-like periodic architectures fabricated by selective laser sintering.", J. Eng. Mater. Technol., Vol. 141, 021009 (2019).

Attarzadeh, R., Rovira, M. and Duwig, C., "Design analysis of the "Schwartz D" based heat exchanger: A numerical study.", Int. J. Heat Mass Transf, Vol. 177, 121415 (2021).

Bicia, M., Brischetto, S., Campanaa, F., Ferro, C. G., Secli, C., Varettib, S., Maggiore, P. and Mazza A., "Development of a multifunctional panel for aerospace use through SLM additive manufacturing." Procedia CIRP, Vol. 67 pp. 215 – 220 (2018).

Castro, A. P. G., Pires, T., Sentos, J. E., Gouveia, B. P., Fernandes, P. R., "Permeability versus Design in TPMS Scaffolds.", Materials (Basel), Vol. 12, 1313 (2019).

Dias, M. R., Fernandes, P. R., Guedes, J.M. and Hollister S.J., "Permeability analysis of scaffolds for bone tissue engineering." J. Biomech., Vol. 45, pp. 938-944 (2012).

Dong, G., Tang, Y. and Zhao, Y. F., "A survey of modeling of lattice structures fabricated by additive manufacturing.", J. Mech. Des., Vol. 139, 100906 (2017).

Fan, H., Sun, F., Yang, L., Jin, F. and Zhao, D., "Interlocked hierarchical lattice materials reinforced by woven textile sandwich composites." Compos. Sci. Technol., Vol. 87, pp. 142-148 (2013).

Fan, H. L., Meng, F. H. and, Yang, W., "Sandwich panels with Kagome lattice cores reinforced by carbon fibers." Compos. Struct., Vol. 81 pp. 533–539 (2007).

Fan, H. L., Zeng, T., Fang, D. N. and Yang, W., "Mechanics of advanced fiber reinforced lattice composites." Acta Mech. Sin., Vol. 26, pp. 825–835 (2010).

Göransson, P., "Acoustic and vibrational damping in porous solids". Philos. Trans. R. Soc. A,, Vol. 364, pp. 89–108 (2006).

Guisheng, Y.,"The select of internal architecture for porous Ti alloy scaffold: A compromise between mechanical properties and permeability". Mater. Des., Vol. 192, 108754 (2020).

Jafari D., Wits, W. W., and Geurts, B. J., "Metal 3D-printed wick structures for heat pipe application: Capillary performance analysis". Appl. Therm. Eng. Vol. 143, Pages 403-414 (2018).

Jung, Y., Chu, K. T. and Torquato, S., "A variational level set approach for surface area minimization of triply-periodic surfaces.", J. Comput. Phys., Vol. 223, pp. 711-730 (2007).

Klinowski, J., Mackay, A. L. and Terrones, H., "Curved surfaces in chemical structure.", Philos. Trans. R. Soc. A, Vol. 354, pp. 1975-1987 (1996).

Kooistra, G.W., Deshpande, V. S. and, Wadley, H.N.G., "Compressive behavior of age hardenable tetrahedral lattice truss structures made from aluminium." Acta Mater., Vol. 52, pp. 4229-4237 (2004).

Leary, M., "Selective laser melting (SLM) of AlSi12Mg lattice structures.", Mater. Des., Vol. 98, pp. 344-357 (2016).

Li, Z., Chen, Z., Chen, X. and Zhao, R., "Design and evaluation of TPMS-inspired 3D-printed scaffolds for bone tissue engineering: Enabling tailored mechanical and mass transport properties.", Compos. Struct, Vol. 327, 117638 (2024).

Li, W., Sun, F., Wang, P., Fan, H. and Fang, D., "A novel carbon fiber reinforced lattice truss sandwich cylinder: Fabrication and experiments." Compos. Part A Appl. Sci. Manuf., Vol 81, pp. 313-322 (2016).

Maskery, I., Aboulkhair, N.T., Aremu, A. O., Tuck, J. and Ashcroft, I. A., "Compressive failure modes and energy absorption in additively manufactured double gyroid lattices.", Addit. Manuf., Vol. 16, pp.24–29 (2017).

Montazerian, H., Zhianmanesh, M., Davoodi, E., Milani, A. S. and Hoorfar, M., "Longitudinal and radial permeability analysis of additively manufactured porous scaffolds: Effect of pore shape and porosity". Mater. Des., Vol. 122, pp. 146-156 (2017).

Neovius, E. R., "Bestimmung zweier speciellen periodischen Minimalflächen: auf welchen unendlich viele gerade linien und unendlich viele ebene geodätische Linien liegen.", J.C. Frenckell & Sohn, (1883).

Pennella, F., Cerino, G, Massai, D., Gallo, D., Falvo D'Urso Labate, G., Schiavi, A., Deriu, M. A., Audenino, A. and Morbiducci U., "A Survey of Methods for the Evaluation of Tissue Engineering Scaffold Permeability." Ann. Biomed. Eng., Vol. 41, pp. 2027–2041 (2013).

Queheillalt, D. T., Murty, Y. and Wadley, H.N.G., "Mechanical properties of an extruded pyramidal lattice truss sandwich structure." Scr. Mater., Vol. 58, pp. 76–79 (2008).

Rathore, S. S., Balkrishna Mehta, B., Kumar, P. and Asfer, M., "Flow characterization in triply-periodic-minimal-surface (TPMS) based porous geometries: Part 1 – hydrodynamics.", Transp Porous Media, Vol. 146, pp. 669–701 (2023).

Reint, D. B., "Highlights in the historical development of the porous media theory: Toward a consistent macroscopic theory." Appl. Mech. Rev., Vol. 49, pp. 201-262 (1996).

Santos, J., Pires, T., Gouveia, B. P., Castro, A. P. G. and Fernandes, P. R., "On the permeability of TPMS scaffolds.", Vol. 110, 103932 (2020).

Sarparast, Z., RAbdoli R., Rahbari, A. Varmazyar, M. and Reza Kashyzadehet K., "Experimental and Numerical Analysis of Permeability in Porous Media." Int. J. Eng., Vol. 33, pp. 2408-2415 (2020)

Schröder-Turk, G. E., "The chiral structure of porous chitin within the wing-scales of Callophrys rubi.", J. Struct. Biol., Vol. 174, pp. 290-295 (2011).

Schoen, A. H., "Infinite periodic minimal surfaces without self-intersections", NASA Technical Report D-5541, (1970).

Stupak, P. R. and Donovan, J. A., "Deformation and energy absorption of polymer foams as a function of 2-d indenter and absorber geometries.” , Polym. Eng. Sci., Vol. 34, pp. 857 – 864 (1994).

Tobias Maconachie, T., Tino, R., Lozanovski, B. and Watson, M., “The compressive behaviour of ABS gyroid lattice structures manufactured by fused deposition modelling.” , Int. J. Adv. Manuf. Technol., Vol. 107, pp 4449 – 4467 (2020) .

Wang, X. and Lu, T. J. “Optimized acoustic properties of cellular solids.”, J. Acoust. Soc. Am, Vol. 106 pp. 756–765 (1999).

Wohlers, T., “History of additive manufacturing” Wohlers report 2015, (2015).

Wong, K. V. and Aldo Hernandez, A., “A Review of Additive Manufacturing.”, ISRN Mech. Eng., Vol. 2012, Article ID 208760 (2012).

Yan, C., Hao, L., Hussein, A. and Young, P.,“Ti–6Al–4V triply periodic minimal surface structures for bone implants fabricated via selective laser melting.”, J. Mech. Behav. Biomed. Mater. Vol. 51, pp. 61-73 (2015).

Yao, Y., Qin, W., Xing, B., Sha, N., Jiao, T. and Zhao, Z., “High performance hydroxyapatite ceramics and a triply periodic minimum surface structure fabricated by digital light processing 3D printing.”, J. Adv. Ceram., Vol. 10, pp.39–48 (2021).

Yu, S., Sun, J., Bai, J., “Investigation of functionally graded TPMS structures fabricated by additive manufacturing.”, Mater. Des., Vol. 182, 108021 (2019).

Zhianmanesh, M., Varmazyar, M. and Montazerian, H., “Fluid permeability of graded porosity scaffolds architectured with minimal surfaces.”, ACS Biomater Sci Eng, Vol. 5, pp.1228-1237 (2019).

Zhu, X., Wang, S., Feng, Q., Zhang, L., Chen L. and Tao, W., “Pore-scale numerical prediction of three-phase relative permeability in porous media using the lattice Boltzmann method.” Int. Commun. Heat Mass Transf.Vol. 126, 105403 (2021).

NOMENCLATURE

A	area of fluid domain Inlet diameter, m^2
D_h	hydraulic diameter, m^2
L	structure length, m
Q	volumetric flow rate, m^3/s
Re	Reynolds number
U	velocity, m/s
div	the divergence operator
k	permeability, m^2
p	pressure
u	velocity vector
u, v, w	the velocity components
Δp	pressure drop, pa
ρ	density, kg/m^3
μ	dynamic viscosity, kg/m·s

晶格結構在不同流動條件下滲透率之數值研究

Parth Goyal　Sundararaj Senthilkumar
印度蘭馬斯瓦米紀念大學航空太空工程學系

康尚文
淡江大學機與機電工程學系

摘 要

多孔材料在吸震、熱管理、組織工程和減震等應用中至關重要，因此對其進行詳細研究非常有必要。在孔隙結構特徵化中，關鍵參數包括孔隙率、孔隙分佈、類型、孔徑大小、形狀、曲折度、孔隙大小分佈、比表面積和滲透性。本研究數值模擬了兩種三重周期最小曲面（TPMS）結構，Primitive 和 Gyroid，以及兩種基於支柱的晶格結構，Diamond 和 Iso-truss 的滲透性。分析在穩態下進行，變化孔隙率（60%、70%、80%、90%）、雷諾數（10、50、100、150、200、250）和側向長度（3 毫米）。結果顯示，較高的孔隙率與較高的滲透性相關，而雷諾數的增加會導致壓降上升，從而降低滲透性。在結構中，晶格結構 Diamond 顯示出最高的滲透性，而 TPMS 結構 Primitive 則普遍具有最低的滲透性。